Effect of Analyst Segmentation Variability on Computed AAA Stress Distributions

T. Hodge[1*], J.C.Y. Tan[1*], P.H. Koh[1*], E. Storer[1*], A. Huynh[1], F. Alkhatib[2], K. Miller[2], A. Wittek[2]

School of Engineering, Computing & Mathematics. The University of Western Australia. Perth, Australia.

Abstract. Abdominal Aortic Aneurysms (AAA) are a symptomless condition and are common in the geriatric population (65< years old). It is imperative for clinicians to identify regions of the AAA with greatest risk of rupture as well as overall rupture risk. A more dependable, patient specific approach based on computational biomechanics which could prove useful. This research paper aims to identify and evaluate the extent of user variability during semi-automatic segmentation providing the geometry for a model. We used patient data obtained from Fiona Stanley Hospital in Perth, Western Australia, in the form of CT scans at 80% through the cardiac cycle. Individual segmentations were performed by four analysts of similar experience with a repeat segmentation conducted four weeks later. Segmentations by different analysts produced different stress results and therefore affected the rupture potential prediction. Segmentations by the same analyst were not exactly reproducible. We recommend more stringent guidelines to guide analysts while utilizing an automated segmentation process by edge detection may also prove to be feasible.

Keywords. Computational biomechanics • Computed tomography • Aneurysms • Segmentation variability • Principal stresses • Canny edges

1. Motivations

An Abdominal Aortic Aneurysm (AAA) is clinically defined as the permanent and irreversible dilation of the abdominal region in the descending aorta. Aneurysm names are characterised by their location, for this project we have investigated aneurysms originating below the renal arteries and are appropriately referred to as infra-renal AAA's which can be illustrated in Figure 1 below. This cardiovascular disease is a symptomless condition that is often discovered by coincidence when undertaking other clinical scans such as bladder screening, ultra-sonographies, or other radiography tests. In many cases, the discovery only takes place after rupture

has taken place, hence it's given nickname "The Silent Killer" (Vascular 2022). Rupture of the aneurysm is lethal, and even with swift medical attention and surgical intervention, the long-term post-operative mortality rates remain high between 30-45% (De Bruin et al. 2010, Greenhalgh et al. 2010). On a global scale, AAA's cause approximately 200,000 deaths per year highlighting its severity (Naghavi and al 2015). The disease is more likely to occur if you have a family history of cardiovascular conditions as well as the typical lifestyle related factors consisting of high cholesterol, elevated blood pressure, obesity as well as excessive alcohol and tobacco consumption (Wanhainen, Verzini et al. 2019). Studies have determined that males are more susceptible to incidence, however, females have a higher risk of rupture (Aggarwal et al. 2011, Wanhainen et al. 2019).

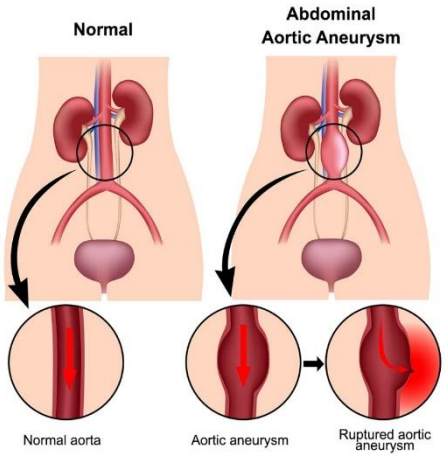

Fig. 1. Infra-renal AAA. Normal and healthy aorta (L). Dilated aortic aneurysm (R). Extracted from: (HealthDirect 2020).

The current gold-standard AAA rupture risk assessment method involves maximum diameter and diameter growth rate (Wanhainen et al., 2019). These criteria prove to be unreliable, as AAAs with diameters smaller than 5.5cm have been shown to rupture, with rates between 7% and 23%. (Darling et al., 1977) While larger AAAs have remained stable (Droz et al., 2017; Greenhalgh et al., 2004). This poses an issue; these guidelines rely on a one size fits all approach which has little physiological basis, as patient-specific information is unaccounted for. This points to the need for a more reliable indicator of AAA rupture risk that incorporates patient-specific biomechanics (Joldes et al., 2016, Polzer et al., 2020, Vorp & Raghavan, 2000). Our overall objective is to develop and verify a non-invasive, patient-specific biomechanics-based rupture risk assessment for AAA. It is these shortcomings associated with diameter-based assessments of AAAs that provided the initial motivations for this research direction.

This paper specifically aims to investigate and examine the effects of inter- & intra-user segmentation variability on the reproducibility of results from computational biomechanics models. To achieve this, a qualitative visual comparison with associated wall stress values will be observed.

2 Methods

Software utilised was constructed by Intelligent Systems for Medicine Laboratory (ISML) at The University of Western Australia, Biomechanics based Prediction of Aneurysm Rupture Risk (BioPARR) available from: https://bioparr.mech.uwa.edu.au

2.1 Patient Demographic

The abdominal CT scan of one patient was obtained from Fiona Stanley Hospital in Perth, Western Australia for analysis. This CT scan was captured at 80% of the cardiac cycle, which corresponds to the diastolic phase in the abdominal aorta, as there is comparatively less noise in this portion. The patient's systolic and diastolic blood pressure was also recorded and will be used to calculate patient specific mean arterial pressures (MAP). Ethical approvals were obtained from both Fiona Stanley Hospital and the University of Western Australia.

2.2 Image Segmentation

All image segmentations to extract the AAA wall geometry were performed in open source segmentation software, 3D Slicer (Fedorov et al., 2012). Four analysts performed two segmentations each, with segmentations conducted four weeks apart. Stress analysis was performed on each geometry to assess intra- and inter-analyst differences in simulation results resulting from differences in segmentations. Semi-automatic segmentation process is detailed below.

ROI creation and lumen segmentation. We first refined the region of interest (ROI) of the AAA. This was achieved through cropping the CT images from the renal arteries to the iliac bifurcation. The voxels of this ROI were then made isotropic at 0.625mm to simplify smoothing. A threshold was applied to differentiate the lumen from surrounding tissue. As this threshold included areas of the spine and surrounding arteries, manual removal was required to ensure the labelmap only contained the aortic lumen. The resulting labelmap was Gaussian smoothed with a σ factor of one.

AAA segmentation. The AAA including lumen was separated from the surrounding tissue through user-interpreted semi-automatic segmentation in the ROI. Using the FastGrowCut (Fedorov et al., 2012) module in 3D slicer, the AAA including lumen was separated from the surrounding tissue throughout the ROI. However, this model had some inaccuracies which had to be manually corrected to ensure the selected region is representative of the AAA. The resulting labelmap was Gaussian smoothed with an appropriate standard deviation, σ, of two to ensure the surface is optimal for the meshing algorithm without removing important AAA features.

AAA wall extraction. A blood masked label is created, which is the lumen label shrunk by 4 pixels. This blood masked label is subtracted from the AAA label previously created to obtain the AAA wall label. The resulting label is manually checked for errors and corrected. A 3D surface model of the AAA wall is created using the ModelMaker module in 3D slicer, with 100 iterations of Laplacian smoothing and the decimate field set to 0.1. This model can be viewed in Paraview – an open source, multi-platform data analysis and visualisation application (Ahrens et al., 2005). A visual process of this extraction can be seen below in Fig. 2.

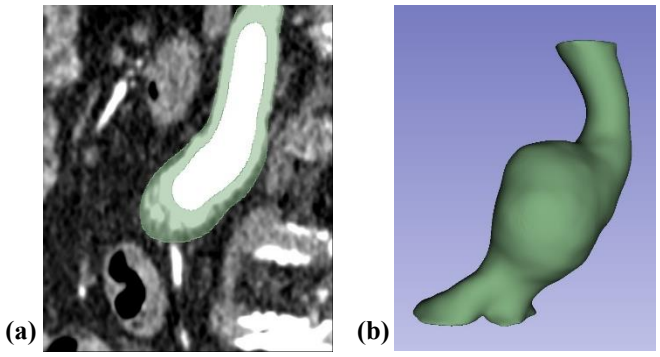

Fig. 2. AAA wall extraction - (a) CT image of AAA wall segmentation viewed in sagittal plane; (b) 3D label reconstruction of AAA wall. Viewed in 3D slicer**.**

2.3 Wall Thickness Specification

AAA wall thickness is an important factor affecting the stress magnitude within the wall. However, accurate determination of wall thickness from medical images remains problematic due to low image resolution and poor soft tissue contrast. Leading to inaccurate and unreliable wall thickness measurements from medical images. This is why previous authors implemented a constant AAA wall thickness in their studies (Truijers et al., 2007; Vande Geest et al., 2006). Therefore, a constant wall thickness of 1.5mm is used here to ensure more reliable comparison of intra and inter-user segmentation differences on AAA wall stress. This constant wall

thickness is applied by AAA rupture risk prediction software, BioPARR (Joldes et al., 2017).

2.4 AAA Geometry Creation

The following steps are automated by BioPARR. The AAA model created in 3D slicer contains elements of different sizes and poor aspect ratios, which will be problematic when creating the AAA wall and intraluminal thrombus (ILT) inner & outer surfaces. So, the surface mesh of the AAA model is re-meshed using mesh resampling software ACVDQ (Valette et al., 2016). Then, a custom command line interface (CLI) 3D slicer module is used to generate the AAA wall and ILT surfaces from the resampled geometry. The three surfaces generated are the external and internal AAA surface, and the internal ILT surface. Thickness of the ILT is computed to ensure it has a minimum thickness of 1mm. Local AAA wall and ILT thicknesses are used to compute the mesh element size ensuring the wall thickness can be represented by two layers of elements.

2.5 Mesh Generation for a Finite Element Model

Meshing of the AAA wall and ILT surfaces are performed using open source meshing software, Gmsh (Geuzaine & Remacle, 2009). The surfaces are first meshed using the previously generated element size information. End surfaces are then generated between the external and internal AAA wall, and the internal AAA wall surface and ILT, to ensure that the surfaces of the geometry are closed and watertight. Using the previously generated element size information, a tetrahedral volumetric mesh is created throughout the geometry. Tetrahedral elements were selected as they better represent complex geometries, such as the bifurcations commonly found in AAAs. Very small tetrahedral elements are generated near the edges of the geometry to maintain geometry accuracy. While element size is increased in the thicker areas of the AAA wall and middle of the of the ILT to reduce element count and therefore computational cost of the finite element analysis. Figure 3 is an example mesh which illustrates the range of element sizes encountered and its distribution.

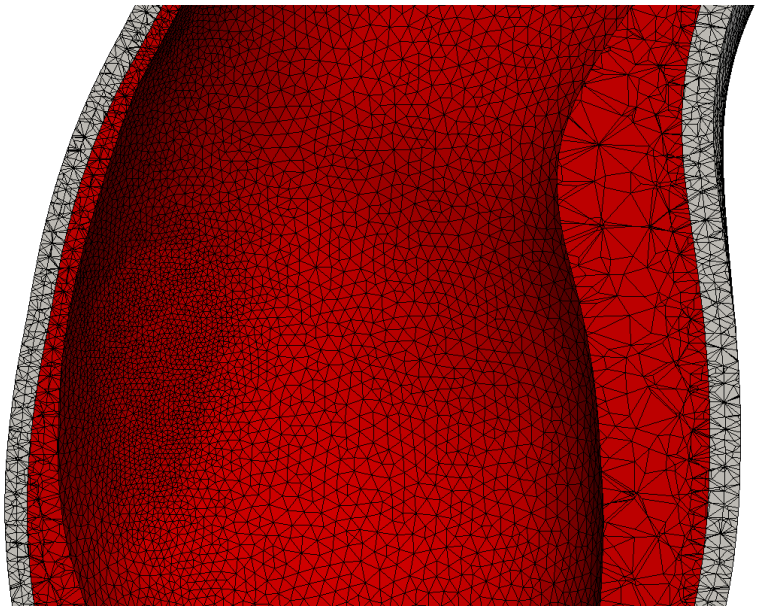

Fig. 3. Generated volume mesh with two layers of AAA wall. Minimum of two elements on ILT wall with larger element sizes inside ILT. Inner layer (red), outer layer (grey).

2.6 Finite Element Model Creation

The previously created volumetric mesh files of the AAA wall and ILT are used to generate input files for commercial finite element software, Abaqus (*Abaqus/CAE User's Manual*, n.d.), using a custom CLI 3D Slicer module. The input files contain the AAA wall and ILT meshes as parts, on which loads, and boundary conditions can be applied. Three loading scenarios are generated, which includes ILT pressure, Wall pressure and No ILT. These scenarios are represented in Figure 4 below. Only results of the ILT pressure scenario will be presented, as this most closely resembles in vivo conditions. The load is the mean arterial pressure determined from patient specific systolic and diastolic blood pressure. While the boundary conditions are that the AAA is tethered superiorly and inferiorly at the renal arteries and iliac bi-furcation respectively to simulate in vivo conditions.

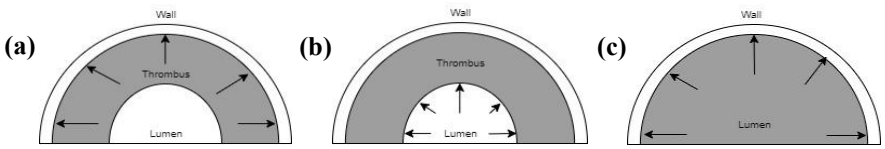

Fig. 4. Loading scenarios used in BioPARR pipeline (a) ILT pressure; (b) Wall pressure; (c) No- ILT.

2.7 Finite Element Analysis

BioPARR calls on ABAQUS to perform finite element analysis of the previously created scenarios, following the procedure of Joldes et al (2016). As the geometry extracted from the CT image is the AAA deformed under patient specific blood pressure, the stress within the AAA wall balances the blood pressure load in that deformed configuration. Therefore, the computed stresses depend on geometry and load, but only very weakly on patient specific wall material properties as demonstrated in (Joldes et al 2016, Miller and Lu, 2011). In essence, results of (Joldes et al 2016, Miller and Lu 2011) demonstrate that an AAA seen in a deformed configuration is approximately a statically determinate structure. This means the stress within the AAA wall balances the blood pressure load, while only being very weakly dependent on patient specific wall material properties. BioPARR ensures the deformed AAA geometry is unchanged under realistic blood pressure load by specifying an aortic Young's modulus of 100 MPa.

Residual stress incorporation. According to the uniform stress hypothesis, residual stress arises from the continual remodelling of arteries, and works to make stress distribution within the vessel wall more uniform under normal conditions (Fung, 1991). To incorporate residual stresses, the previously extracted max principal stress is averaged over the AAA wall thickness (Joldes et al., 2018). This is performed for each node on the AAA wall surface to extract the max wall stress under the uniform stress hypothesis.

99th percentile max principal stress. After extraction of max principal wall stress, the 99th percentile max principal stress is calculated via MATLAB. The 99th percentile is an arbitrary number used to remove any inaccurate peak stresses due to meshing artefacts (Speelman et al., 2008). These 99th percentile values will be used to compare intra and inter-analyst variability.

2.8 Evaluating Intra- & Inter-analyst Segmentation Variability

To evaluate the differences in inter-analyst segmentation, all four analysts individually segmented one patient, Patient 34, as a control. The completed segmentations followed the same protocols defined in 2.2 to generate geometry and compute wall stresses. The maximum principal stress of each geometry is extracted, from which the peak and 99th percentile max principal stresses are computed and graphically visualized in Matlab and Paraview. These stress values allow comparison of each geometry, its segmentation, and their effects on computed AAA wall stress, which may be clinically significant. Two sets of data per analyst was obtained, as each analyst performed the process four weeks apart. From these two sets of data per analyst, the intra-analyst segmentation variability and its effects on computed stress can be assessed. The segmentations were input to BioPARR to compute AAA wall stress. The wall stress was used as a metric to compare the effects of segmentation variability arising from the same analyst on the same patient.

3. Results

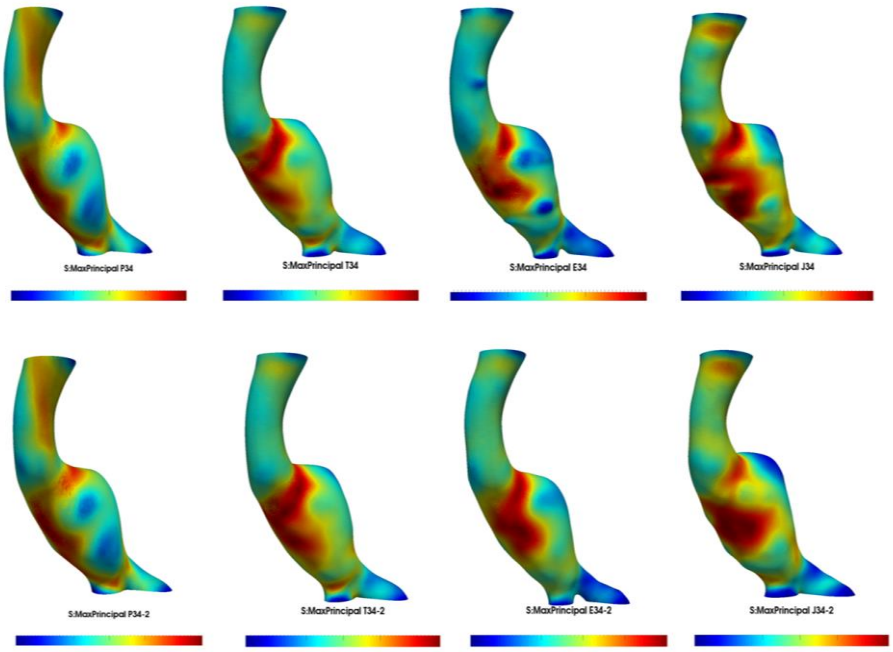

Fig. 5. Stress field contour plots of patient 34 on the same scale for each user. Attempt one (top) and second attempt (bottom). E34-1 has a significantly higher stress field than the other models. Regions of high stress are localized to high curvature areas that are similar across all geometries, although their stress values are different. All models viewed in Paraview.

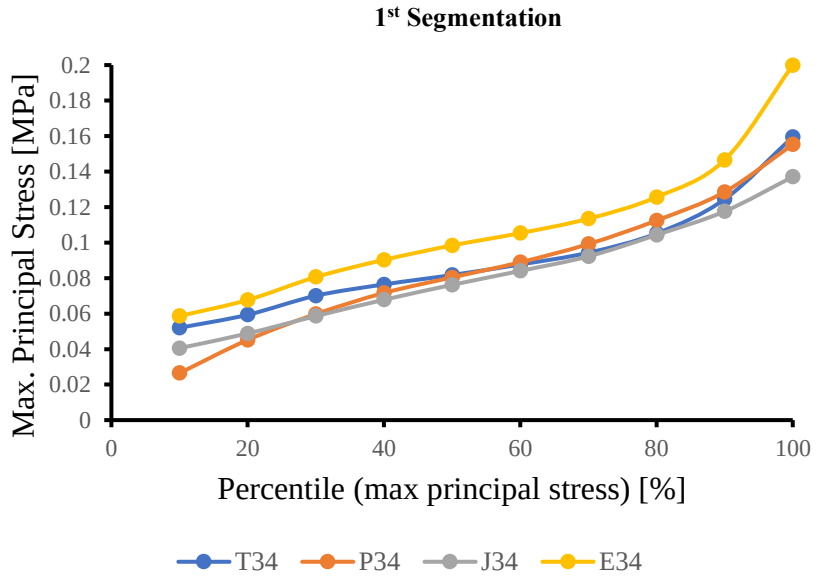

Fig. 6. Percentile plot of maximum principal stresses for 1st segmentation of patient 34. Relative variability in stress values between users. 99th percentile values for T34 = 0.2256 MPa, P34 = 0.2282 MPa, J34 = 0.1417 MPa and E34 = 0.2669 MPa.

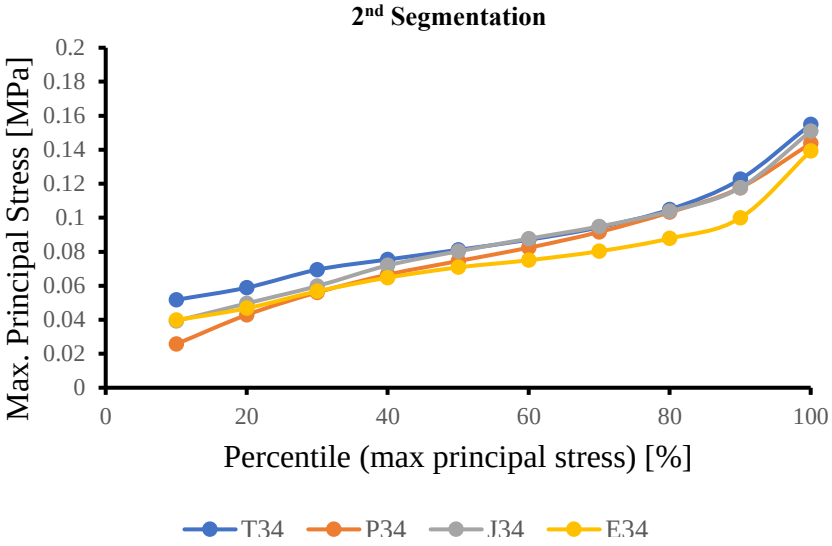

Fig. 7. Percentile plot of maximum principal stress for 2nd segmentation of patient 34. Maximum value is T34 at 0.168MPa. There still exists a relative difference in the stress values between users. 99th Percentile values for T34 = 0.2156 MPa, P34 = 0.2548 MPa, J34 = 0.1682 MPa, and E34 = 0.1416 MPa.

3.1 Inter-user Segmentation

Tables 1 & 2 present results of patient 34 from segmentations by four different analysts. The peak 99th percentile and average maximum principal stresses are presented along with the number of nodes per geometry. From these tables we can appreciate a difference of 0.125MPa between the greatest and lowest 99th percentile maximum principal stresses. For segmentation 1, the 99th percentile stresses diverged from the average by 23.79% for E34, 34.28% for J34, 5.84% for P34 and 4.64% for T34. Interestingly from the percentile plots of Figures 6 & 7, graphically, there is a larger spread of inter-analyst results in the first segmentation than is shown in the second segmentation. Figure 5 presents regions of high wall stress of the AAA, which are all localized to the same regions for all analysts. These regions of high stress are localized to the high curvature areas across all geometries despite their stress value differences.

Table 1. Peak 99th percentile and average maximum principal stresses of the first inter-analyst segmentations. Number of nodes contained in the geometry are also presented. Percentage differences are calculated relative to the means of each metric.

Segmentation 1						
Analyst	**Peak stress (MPa)**	**99th percentile stress**		**Average stress (MPa)**	**No. of nodes**	
		Value (MPa)	**Difference (%)**		**Value**	**Difference (%)**
E34	0.4229	0.2669	23.79 %	0.1008	146,808	7.93 %
J34	0.2479	0.1417	-34.28 %	0.0691	145,892	7.26 %
P34	0.7766	0.2282	5.84 %	0.0696	101,252	-25.56 %
T34	0.3445	0.2256	4.64 %	0.0853	150,125	10.37 %
Average		0.2156			136,019	

Table 2. Peak 99th percentile and average maximum principal stresses of the second inter-analyst segmentations. Number of nodes contained in the geometry are also presented. Percentage differences are calculated relative to the means of each metric.

Segmentation 2						
Analyst	Peak stress (MPa)	99^{th} percentile stress		Average stress (MPa)	No. of nodes	
		Value (MPa)	Difference (%)		Value	Difference (%)
E34	0.2568	0.1416	-27.40 %	0.0691	145,663	6.44 %
J34	0.2253	0.1682	-13.77 %	0.0776	148,862	8.77 %
P34	0.6440	0.2548	30.63 %	0.0750	103,846	-24.12 %
T34	0.3627	0.2156	10.54 %	0.0845	149,042	8.91 %
Average		0.1951			136,853	

3.2 Intra-user Segmentation

Between Tables 1 & 2 and Figures 5-7 we are also able to observe the results the two segmentations conducted four weeks apart. Peak 99^{th} percentile and average maximum principal stresses are presented along with the number of nodes. The largest differences in 99^{th} percentile stresses were of E34 and J34, of which decreased by 30.67% and 8.55% respectively. While P34 and T34 only exhibited small relative stress differences at 5.51% and 2.27% respectively. The stress percentile plots of Figures 6 & 7 demonstrate similar patterns for distribution of wall stress over percentiles for all four analysts. However, E34 and J34 presented large stress differences in segmentation two compared to one, while P34 and T34 remained very similar. Figure 5 also illustrates that high stress locations remain the same for both segmentations of E34 and J34, whilst the stress magnitudes differ considerably. Alternatively, P34 and T34 exhibit similar stress locations and stress magnitudes.

4. Discussion

The CT images that were segmented had voxel sizes of 0.625mm cubed. By nature, CT imaging has difficulties capturing and visualising low-contrast structures like soft tissue. As the AAA is primarily made up of and surrounded by soft tissue, identification of the AAA compared to surrounding tissue may vary among users. Assuming an uncertainty of two pixels on each edge, there is a potential difference of up to 2.5mm in model generation. While this may seem like a small value, it is

important to consider that 3D-CT images contain a stack of 2D images which will compound on the uncertainty of each slice.

Considering that the generated 3D model is crucial for the results, it can be observed from Figures 5-7 that there is variability among users. This variability can cause influential differences in the resulting regions of wall stress. Additionally, the team decided to test if there was intra-user variability. After four weeks from the initial model generation of patient 34, the team conducted another segmentation of the AAA from patient 34. The results from all four analysts are illustrated in Figure 5 which shows the presence of intra-user variability for each team member. It is important to note that all team members are of relatively equal experience and followed the same protocol when producing segmentations. This further reinforces the need to have a standardised way to segment AAA models in patients to eliminate the variability that can arise from both inter- & intra-user sources.

There are limitations to this study, however. The first being that the computed stress values demonstrated here cannot be validated by realistic, in vivo results, as no experimental results of AAA wall stress are available. Therefore, no conclusions can be made regarding the accuracy of the results obtained here. The wall stresses computed here are also potentially unreliable in AAA rupture risk prediction, as no patient specific wall strength metric is available to compare local wall stresses and strengths. The assumption of a constant, 1.5mm AAA wall thickness used here presents as a limitation, as it does not represent patient-specific AAA geometry. Inaccuracies of the computed stress in the AAA wall will arise, as maximum principal stresses are proportional to the wall thickness (Miller et al., 2019). This study does verify however, the presence of user variability. Whilst differences between the 99th percentile maximum principal stresses were minimal (less than 8.55%) for three out of the four analysts, one analyst (E34) reported a 30.67% difference between computed stresses. In addition to this, two out of the four analysts reported slight changes in the locations of high stress on the AAA wall.

4.1 Canny Edge Detection – Future Implications

Edge detection algorithms are widely used in image processing and image analysis, especially when identifying objects within an image and preserving structural information about object boundaries. Most edge detection algorithms only require parametric user input to detect object boundaries and can be used as an alternative to semi-automatic free-hand segmentation such as FastGrowCut within 3D Slicer. Although FastGrowCut has the advantage of providing users with an interactive segmentation method that is effective and efficient over other manual methods, the method requires large amounts of user input by manually drawing seeds and background pixels to guide the segmentation (Zhu et al., 2014) and may be a contributing factor to the intra- and inter-analyst variability. As such, edge detection algorithms

such as Canny edge detection (Canny, 1986) where users are required to input parameters for Gaussian smoothing and thresholding instead of manual segmentation may reduce variability. Figure 8 below shows a sample of the aortic wall detected by the Canny edge detection algorithm available in MATLAB. This method has been applied to previous work on detecting and measuring AAA wall thickness (Huynh & Miller, 2022) and has the potential to be used as guidance in the form of object edge boundaries for image segmentation, reducing intra- and inter-analyst variability. Further advancements into edge detection needs to be investigated, with Canny edge detection being a simple, yet effective example of its application in medical imaging analysis.

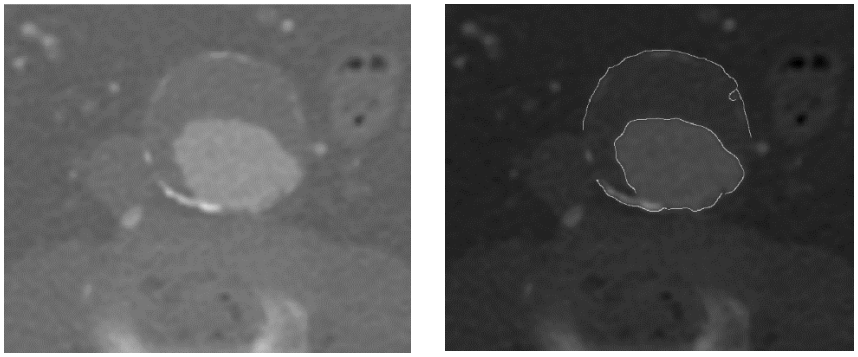

(a) (b)

Fig. 8. Example of Canny edge detection for guiding image segmentation of the abdominal aortic aneurysm from CT scans. (a) Original axial CT slice (b) CT slice with Canny edges (in white).

5. Conclusion

This study verifies the workflow of AAA rupture risk prediction software, BioPARR, by analyzing nine patients. The stresses computed by BioPARR and Abaqus present high stresses in region of large curvature. BioPARR was utilized to analyze the inter- and intra-analyst segmentation variability and its effects on computed stress fields. Differences were observed when comparing segmentations performed by the four analysts, with the number of nodes in the geometry being different. Additionally, the location of high stress areas differs slightly between the segmentations. These factors directly affect the prediction of rupture risk occurrence and location. Future studies are recommended to incorporate Bland & Altman's difference of mean methods and plots to obtain a more reliable comparison of intra- & inter- user segmentation differences and their effects on computed wall stresses. This paper also highlights the importance of the development of edge detection methods which reduce user variability altogether.

References

Abaqus/CAE User's Manual. (n.d.). 1174.

Aggarwal, S., A. Qamar, V. Sharma and A. Sharma (2011). "Abdominal aortic aneurysm: A comprehensive review." Experimental and clinical cardiology **16**(1): 11-15.

Ahrens, James, Geveci, Berk, Law, Charles, *ParaView: An End-User Tool for Large Data Visualization*, Visualization Handbook, Elsevier, 2005, ISBN-13: 978-0123875822

Canny, J. "A Computational Approach to Edge Detection," in IEEE Transactions on Pattern Analysis and Machine Intelligence, vol. PAMI-8, no. 6, pp. 679-698, Nov. 1986, doi: 10.1109/TPAMI.1986.4767851.

De Bruin, J. L., A. F. Baas, J. Buth, M. Prinssen, E. L. G. Verhoeven, P. W. M. Cuypers, M. R. H. M. van Sambeek, R. Balm, D. E. Grobbee and J. D. Blankensteijn (2010). "Long-Term Outcome of Open or Endovascular Repair of Abdominal Aortic Aneurysm." New England Journal of Medicine **362**(20): 1881-1889.

Fedorov, A., Beichel, R., Kalpathy-Cramer, J., Finet, J., Fillion-Robin, J.-C., Pujol, S., Bauer, C., Jennings, D., Fennessy, F., Sonka, M., Buatti, J., Aylward, S., Miller, J. V., Pieper, S., & Kikinis, R. (2012). 3D Slicer as an image computing platform for the Quantitative Imaging Network. *Magnetic Resonance Imaging*, *30*(9), 1323–1341. https://doi.org/10.1016/j.mri.2012.05.001

Fung, Y. C. (1991). What are the residual stresses doing in our blood vessels? *Annals of Biomedical Engineering*, *19*(3), 237–249. https://doi.org/10.1007/BF02584301

Geuzaine, C., & Remacle, J.-F. (2009). Gmsh: A 3-D finite element mesh generator with built-in pre- and post-processing facilities: THE GMSH PAPER. *International Journal for Numerical Methods in Engineering*, *79*(11), 1309–1331. https://doi.org/10.1002/nme.2579

Greenhalgh, R. M., L. C. Brown, J. T. Powell, S. G. Thompson, D. Epstein and M. J. Sculpher (2010). "Endovascular versus open repair of abdominal aortic aneurysm." N Engl J Med **362**(20): 1863-1871.

HealthDirect. (2020). "Aortic Aneurysm." 2022, from https://www.healthdirect.gov.au/aortic-aneurysm.

Huynh A., Miller K. (2022). Towards accurate measurement of abdominal aortic aneurysm wall thickness from CT and MRI. In P M.F. Nielsen, M. Nash, X. Li, K. Miller & A. Wittek, *Computational Biomechanics for Medicine - Towards translation and better patient outcomes*. Springer International Publishing.

Joldes, G. R., Miller, K., Wittek, A., & Doyle, B. (2016). A simple, effective and clinically applicable method to compute abdominal aortic aneurysm wall stress. *Journal of the Mechanical Behavior of Biomedical Materials*, *58*, 139–148. https://doi.org/10.1016/j.jmbbm.2015.07.029

Joldes, G. R., Miller, K., Wittek, A., Forsythe, R. O., Newby, D. E., & Doyle, B. J. (2017). BioPARR: A software system for estimating the rupture potential index for abdominal aortic aneurysms. *Scientific Reports*, *7*(1), 4641. https://doi.org/10.1038/s41598-017-04699-1

Joldes, G. R., Noble, C., Polzer, S., Taylor, Z., Wittek, A., & Miller, K. (2018). A simple method of incorporating the effect of the Uniform Stress Hypothesis in arterial wall stress computations [PDF]. *Acta of Bioengineering and Biomechanics; 03/2018; ISSN 1509-409X*. https://doi.org/10.5277/ABB-01143-2018-03

Miller, K. and J. Lu (2013). "On the prospect of patient-specific biomechanics without patient-specific properties of tissues." Journal of the Mechanical Behavior of Biomedical Materials **27**: 154-166.

Miller, K. *et al.* (2019). Maximum Principal AAA Wall Stress Is Proportional to Wall Thickness. In: Nielsen, P., Wittek, A., Miller, K., Doyle, B., Joldes, G., Nash, M. (eds) *Computational Biomechanics for Medicine*. Springer, Cham. https://doi.org/10.1007/978-3-319-75589-2_5

Naghavi, M. and e. al (2015). "Global, regional, and national age–sex specific all-cause and cause-specific mortality for 240 causes of death, 1990–2013: a systematic analysis for the Global Burden of Disease Study 2013." The Lancet **385**(9963): 117-171.

Raghavan, M. L. and D. A. Vorp (2000). "Toward a biomechanical tool to evaluate rupture potential of abdominal aortic aneurysm: identification of a finite strain constitutive model and evaluation of its applicability." Journal of Biomechanics **33**(4): 475-482.

Speelman, L., Bosboom, E. M. H., Schurink, G. W. H., Hellenthal, F. A. M. V. I., Buth, J., Breeuwer, M., Jacobs, M. J., & van de Vosse, F. N. (2008). Patient-Specific AAA Wall Stress Analysis: 99-Percentile Versus Peak Stress. *European Journal of Vascular and Endovascular Surgery*, *36*(6), 668–676. https://doi.org/10.1016/j.ejvs.2008.09.007

Truijers, M., Pol, J. A., Schultzekool, L. J., van Sterkenburg, S. M., Fillinger, M. F., & Blankensteijn, J. D. (2007). Wall stress analysis in small asymptomatic, symptomatic and ruptured abdominal aortic aneurysms. *European Journal of Vascular and Endovascular Surgery: The Official Journal of the European Society for Vascular Surgery*, *33*(4), 401–407. https://doi.org/10.1016/j.ejvs.2006.10.009

Valette, S., M, J., & Prost, R. (2016, April 27). *ACVD: Surface mesh corasening and resampling.* Sébastien Valette. https://www.creatis.insa-lyon.fr/~valette/public/project/acvd/

Vande Geest, J. P., Di Martino, E. S., Bohra, A., Makaroun, M. S., & Vorp, D. A. (2006). A biomechanics-based rupture potential index for abdominal aortic aneurysm risk assessment: Demonstrative application. *Annals of the New York Academy of Sciences*, *1085*, 11–21. https://doi.org/10.1196/annals.1383.046

Vascular, S. V. (2022). "Abdominal Aortic Aneurysms Symptoms, 'The Silent Killer'." 2022, from https://www.southvalleyvascular.com/post/abdominal-aortic-aneurysms-symptoms-the-silent-killer#:~:text=An%20abdominal%20aortic%20aneurysm%20is,abdominal%20aortic%20aneurysm%20than%20women.

Wanhainen, A., et al. (2019). "Editor's Choice - European Society for Vascular Surgery (ESVS) 2019 Clinical Practice Guidelines on the Management of Abdominal Aorto-iliac Artery Aneurysms." Eur J Vasc Endovasc Surg **57**(1): 8-93.

Zhu L, Kolesov I, Gao Y, Kikinis R, Tannenbaum A. An Effective Interactive Medical Image Segmentation Method using Fast GrowCut. Int Conf Med Image Comput Comput Assist Interv. Workshop on Interactive Methods. 2014;17 (WS).